Magnetic interactions and reversal behavior of $Nd_2Fe_{14}B$ particles diluted in a Nd matrix

D. C. Crew,[1,2,*] Er. Girt,[3] D. Suess,[4] T. Schrefl,[4] K. M. Krishnan,[5] G. Thomas,[5,6] and M. Guilot[7]
[1]*Materials and Chemical Sciences Division, Energy Science and Technology Department, Brookhaven National Laboratory, Upton, New York 11973*
[2]*Department of Physics, The University of Western Australia, 35 Stirling Highway, Crawley, WA 6009, Australia*
[3]*Seagate Technology, 47010 Kato Road, Fremont, California*
[4]*Institute of Applied and Technical Physics, Vienna University of Technology, Haupstr. 8–10, A–1040 Vienna, Austria*
[5]*Materials Science Division, Lawrence Berkeley National Laboratory, Berkeley, California 94720*
[6]*Department of Material Science and Engineering, University of California, Berkeley, California 94720*
[7]*Laboratoire des Champs Magnétiques Intenses, CNRS/MPI, 38042 Grenoble, France*
(Received 6 June 2002; published 18 November 2002)

Reversible magnetization measurements, micromagnetic modeling, the temperature dependence of coercivity, and magnetic viscosity measurements have been used to clarify the magnetic reversal mechanism of $Nd_2Fe_{14}B$ particles contained in a Nd matrix. The coercivity was observed to increase markedly as the dilution of the $Nd_2Fe_{14}B$ phase was increased. The increase in coercivity was accompanied by a change in the reversal mechanism. In the least dilute samples, domain wall motion involving several grains governed by intergrain interactions was active. In the most dilute samples nonuniform reversal of individual grains was dominant, reversal occurring particle by particle and resembling the behavior of isolated Stoner-Wohlfarth particles. The value of the coercivity in the most dilute sample was in excellent agreement with micromagnetic modeling results for isolated particles when the effect of thermal activation of magnetization reversal was accounted for. Despite the single particle reversal mechanism of the most dilute samples, a linear dependence of coercivity on packing fraction was not observed. This is attributed to a clustering of the grains in the samples and changes in grain shape with composition. In all samples, regardless of dilution, the initial magnetic state after thermal demagnetization was found to be one in which a substantial proportion of grains were in a multidomain state. However, micromagnetic simulations for isolated particles of similar shape to those in the most dilute sample showed that the single domain state is the lowest energy state. It is concluded that thermal demagnetization can result in the system remaining in a local metastable state and not the global energy minimum. Micromagnetic calculations showed that one or more domain walls can arise in a grain during thermal demagnetization and that magnetostatic effects provide a significant energy barrier in zero field to the removal of a domain wall once it is formed.

DOI: 10.1103/PhysRevB.66.184418 PACS number(s): 75.60.Jk, 75.50.Tt, 75.50.Vv

I. INTRODUCTION

The study of interaction effects in magnetic systems consisting of small particles is of interest from the point of view of using such systems as a probe of the fundamental physics of magnetic interactions, as well as from the technological standpoint of understanding interacting fine particle systems such as magnetic recording media.

Previous theoretical works on granular magnetic solids consisting of ferromagnetic particles embedded in a nonmagnetic matrix have shown that magnetic interactions have a strong effect on the coercivity. Néel[1] found, by a simple energy argument, that magnetostatic interactions should decrease the coercivity linearly as the concentration of ferromagnetic particles increases. Wohlfarth[2] went on to rigorously derive, for certain particle arrangements, the magnetostatic interaction between particles which reverse by coherent rotation. He found that the leading term for the coercivity, although not identical to Néel's, decreases linearly with increase in packing fraction. The slope of the linear relationship between coercivity and packing fraction was found to be a function of the geometrical arrangement of particles. El Hilo *et al.*[3] used a numerical simulation to examine the effect of concentration on coercivity for coherently rotating, randomly oriented, randomly placed particles, including exchange and magnetostatic interactions. They found the variation of coercivity with packing fraction to be nearly linear for fractions less than 0.4, suggesting in general that higher order terms are not important.

Recently a series of samples have been made by the melt-quenching technique using a starting alloy consisting of $Nd_xFe_{13.1}B$ where x is 2.05, 6, 38.1, or 147.6,[4,5] which ranges from slightly Nd rich compared with the stoichiometric composition to containing atomically over 90% Nd. In the as-quenched condition the samples are amorphous. Appropriate annealing treatments result in the formation of $Nd_2Fe_{14}B$ grains with dimensions in the tens of nanometers, separated to varying degrees by a crystalline, paramagnetic Nd matrix. The amount of the matrix phase depends on the degree of enrichment of Nd in the starting alloy compared with stoichiometric $Nd_2Fe_{14}B$. These samples are all slightly enriched in boron compared with the stoichiometric alloy, but this does not have a large effect on the coercivity.[5] The coercivity has been found to increase markedly with increasing dilution, but the variation is not linear.[5] One analysis[6] has shown that coercivity may vary linearly with average particle separation rather than concentration.

These samples provide an ideal experimental material to

TABLE I. Sample label, sample compositions and annealing treatment for the samples examined.

Sample label	Composition	Annealing treatment
2	$Nd_{2.05}Fe_{13.1}B$	4 min at 973 K
6	$Nd_6Fe_{13.1}B$	2 min at 873 K
38	$Nd_{38.1}Fe_{13.1}B$	4 min at 823 K
147	$Nd_{147.6}Fe_{13.1}B$	4 min at 823 K

examine interaction effects between grains and to examine the changes in the magnetization reversal mechanism which occur as the level of interactions between grains is reduced. There are two main intergranular interactions which change in magnitude and effect as the dilution is increased; exchange interactions, which are short ranged and required close contact between grains, and dipolar interactions, which are comparatively long ranged and can penetrate nonmagnetic or paramagnetic material. The changing importance of each of these interactions as dilution is increased is one reason the coercivity does not vary linearly over the full range of concentration.

This paper reports on a series of magnetic measurements performed on these samples. Of interest was how the magnetization reversal mechanism changed as magnetic interactions decreased and how close the ideal non-interacting small particle limit, typified by the theory of Stoner and Wohlfarth,[7] could be approached. While behavior displaying all aspects of the ideal limit was not observed, the deviation from the idealized behavior in the sample of greatest dilution can be explained with the aid of both two- and three-dimensional micromagnetic calculations. The coercivity as a function of dilution was not found to obey the ideal relationship of Néel over the whole range of packing fraction investigated but rather two different regimes of behavior were observed. Also found was that the thermal demagnetization of the most dilute sample did not result in a global energy minimum state being reached. Rather a metastable equilibrium was established, separated from the global energy minimum by a significant energy barrier caused by magnetostatic interaction.

II. EXPERIMENTAL RESULTS

A. Sample Preparation

The $Nd_xFe_{13.1}B$ ($2.05 \leqslant x \leqslant 147.6$) alloys, prepared by arc melting, were melt spun in an argon atmosphere using a copper wheel with a surface speed of 35 m/s. For ease of description the four samples will be labeled by their Nd content, as shown in Table I along with the annealing treatments applied to the samples to achieve optimum coercivity. These are the same annealing treatments for samples of the same composition used by Girt *et al.*[5] except for sample 2, which was annealed at a higher temperature in this work, 973 K compared with 923 K for Girt *et al.*[5] The as-quenched and annealed ribbons were characterized previously by differential scanning calorimetry, x-ray diffraction, thermomagnetic analysis, and transmission electron microscopy (TEM).[4,5,8]

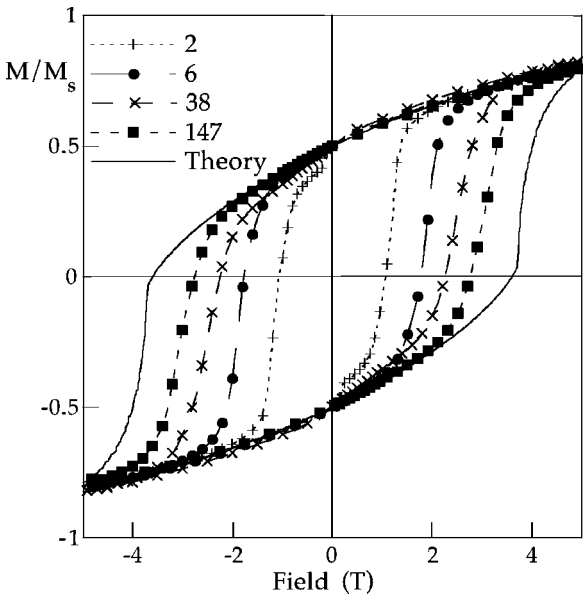

FIG. 1. Hysteresis loops at room temperature, as well as an idealized isotropic ensemble of coherently rotating particles, denoted ''theory'' in the figure. The paramagnetic contribution from the Nd matrix has been subtracted.

Results show that by changing the Nd concentration, the ratio between the $Nd_2Fe_{14}B$- and Nd-rich matrix can be systematically controlled. The extensive previous work on this system is one reason it is of interest for fundamental magnetic studies.

B. Hysteresis

Magnetization measurements were performed in the temperature range from 300 to 550 K using a maximum external applied field up to 5.5 T in a superconducting quantum interference device magnetometer. For measurements below room temperature an extraction method was used with fields up to 23 T. The hysteresis loops for samples 6, 38, and 147 contain contributions from the ferromagnetic $Nd_2Fe_{14}B$ phase and paramagnetic Nd-rich phases. The paramagnetic contribution for each sample was determined from high field measurements above the anisotropy field of $Nd_2Fe_{14}B$, where the magnetization of the $Nd_2Fe_{14}B$ phase is constant. The paramagnetic contribution was in good agreement with the paramagnetic contribution of α-Nd, and was subtracted from the data for all subsequent analysis. The samples were in the form of thin ribbons measured parallel to the ribbon direction so demagnetizing corrections were negligible.

Room temperature hysteresis loops for the four samples, together with an idealized hysteresis loop for isotropic particles of $Nd_2Fe_{14}B$ reversing by coherent rotation,[7] are shown in Fig. 1. The idealized hysteresis loop assumes isolated particles and accounts only for the magneto-crystalline anisotropy, neglecting particle shape effects. It can be observed that as the degree of dilution increases, the hysteresis loop approaches more closely that of idealized coherent rotation. However, even in the most dilute sample the coercivity is some 0.8 T below that of idealized $Nd_2Fe_{14}B$ particles.

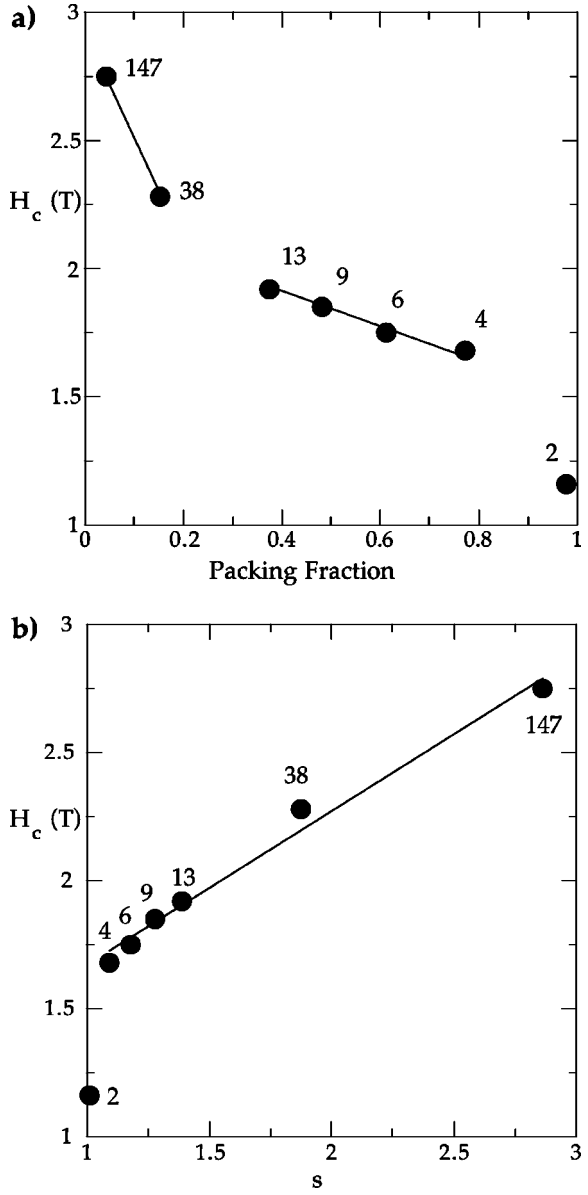

FIG. 2. Coercivity as a function of Nd composition in $Nd_xFe_{13.1}B$ for the samples measured in this work, as well as some similar samples measured in previous work of Ref. 5 The numbers on the figures refer to the sample number from Table I. For samples not listed in Table I the Nd composition x is used as the label. (a) Coercivity as a function of packing fraction. Lines are drawn as a guide to the eye. (b) Coercivity as a function of linear particle separation (as defined by Ref. 6). The line shown is a line of best fit to all the data excluding sample 2.

Figure 2(a) shows the coercivity as a function of packing fraction for the four samples measured, together with additional points for similar samples from previous work.[5] It can be seen that the linear relationship predicted by Néel,[1] does not exist over the whole range of packing fraction investigated. For comparison Fig. 2(b) shows the coercivity for the same samples as a function of average linear separation as defined by Woodward *et al.*[6] This figure shows a much more nearly linear relationship over almost the whole range of packing fraction measured, in accord with the measurements

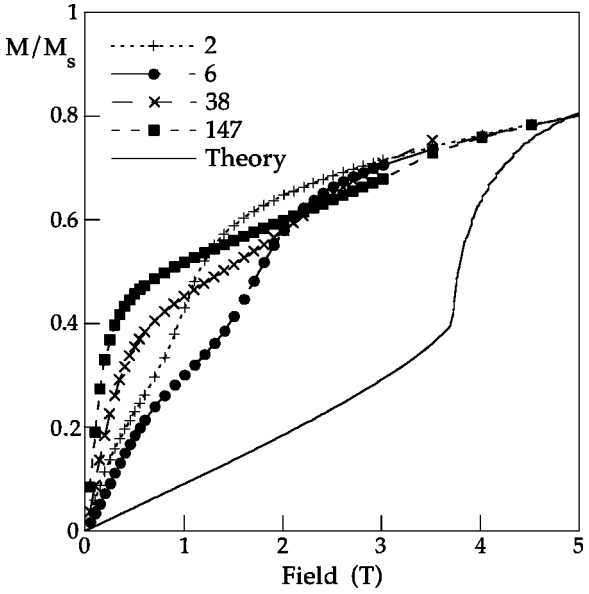

FIG. 3. Initial curves at room temperature from the thermally demagnetized state for the samples shown in Fig. 1, along with the idealized isotropic Stoner-Wohlfarth curve ("theory"). The paramagnetic contribution from the Nd matrix has been subtracted.

of Woodward *et al.*[6] on similar samples. It should be noted that such a relationship has no current theoretical basis.

The initial curves for the samples, including the idealized curve for comparison, are shown in Fig. 3. On the initial curve the behavior of all the samples is very different to that of the idealized theory. The initial curves show a rapid increase in magnetization in low fields. For samples 2 and 6 these curves resemble those measured in melt-quenched NdFeB magnets[9] with two steps on the curve, associated with single and multidomain grains reversing. For samples 38 and 147 the curves resemble those of sintered NdFeB (Ref. 9) with a large low field step, although a second small high field step is also present. From the initial curves it can be determined that in all samples domain walls are present in at least some of the grains in the thermally demagnetized state. The proportion of grains containing domain walls in the thermally demagnetized state increases with particle dilution.

These measurements are in agreement with previous work,[4,5] except for sample 2, which for a different annealing treatment was found to display only single domain initial curve behavior.[5] In this work sample 2 has been subject to a higher annealing temperature compared with that in Girt *et al.*,[5] and it is expected that some grain growth may have occurred. This is the likely reason for the presence of multidomain grains observed for sample 2 in this work compared with their absence in the work of Girt *et al.*[5]

1. Transmission electron microscopy

Previous TEM work[5] showed that, for nearly single phase $Nd_2Fe_{14}B$ prepared by the same method as the samples in this work, the grains are randomly oriented, polyhedral and with an average size between 50 and 70 nm. Diluting the sample with a higher Nd content promotes the growth of the $Nd_2Fe_{14}B$ grains into an elongated shape.[5] For the less dilute

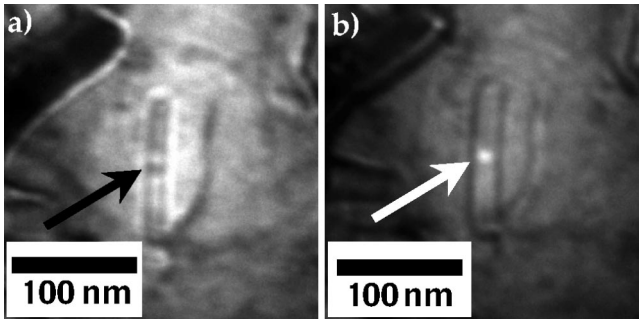

FIG. 4. Lorentz TEM image, using the Fresnel imaging method, of a grain in sample 147 showing a domain wall within the grain in the thermally demagnetized condition (marked by the arrows). (a) Underfocused image. (b) Overfocused image. Fresnel imaging involves slightly under focusing or overfocussing the image to reveal magnetic domain wall contrast so the grain image is slightly blurred in both cases. Note that the contrast of the domain wall changes between the two images which is indicative that it is magnetic in nature.

samples, 2 and 6, many grains are close to each other and intergranular contact at grain boundaries is common. For the more dilute samples, 38 and 147, the grains are elongated, typical dimensions for sample 147 being $100\times40\times25$ nm^3 with the easy axis parallel to the short side of the grain. The grains are randomly oriented and most are isolated from neighboring grains by the Nd matrix, with only the occasional cluster of grains observed, less so in sample 147 than in sample 38.[5]

These previous results on grain size and distribution suggest that the grains in the most dilute samples (38 and 147) are too small to support domain walls in the thermally demagnetized state. In this work Lorentz microscopy was performed in a Philips CM200 FEG microscope using the Fresnel imaging method to investigate the multi-domain structure deduced to be present from the initial curve of the most dilute samples. In this imaging method, domain walls provide the magnetic contrast. The imaging was performed with the objective lens switched off to minimize the magnetic field in the sample area. In order to obtain high magnification, a Gatan Imaging Filter with a CCD camera was used. In Fig. 4 Fresnel images of the multidomain structure of $Nd_2Fe_{14}B$ grains in sample 147 are shown. The domain wall is formed perpendicular to the longest side of the platelet-like grain. Note that the domain wall width is less than 5 nm in $Nd_2Fe_{14}B$,[10] and is close to the resolution limit of the microscope. Despite this, Fig. 4 clearly shows the multidomain structure of these grains.

A variety of magnetic measurement techniques were used to investigate the reversal mechanism of the samples to examine how the magnetic behavior changed with increasing dilution. These techniques included measurement of hysteresis (shown above), reversible magnetization, magnetic viscosity, and the temperature dependence of the coercivity and remanence.

2. Reversible magnetization

Reversible magnetization (M_{rev}) is defined as the change in magnetization upon removal of the field while irreversible magnetization (M_{irr}) is defined as the remnant magnetization once the field is removed. An analysis of reversible magnetization, as described by Crew *et al.*,[9] was conducted at room temperature on both the initial curve and the demagnetization curve. Recoil curves to zero field from a variety of fields along the initial curve and the demagnetization curve were measured for each sample. From these recoil curves the dependence of M_{rev} on M_{irr} at a fixed magnetic field was calculated using the method described by Crew *et al.*[9] Plots of this dependence are known as reversible magnetization curves, and the shape is indicative of the magnetization reversal mechanism. This dependence can be described by a parameter η which is defined as[11]

$$\eta=\left.\frac{dM_{rev}}{dM_{irr}}\right|_H, \tag{1}$$

and is equivalent to the slope of the reversible magnetization curves. Normally η is calculated at the point on the reversible magnetization curve nearest the positive M_{irr} end, as this point is closest to the major hysteresis curve or initial curve (as appropriate) and is the point of greatest interest.

For the major hysteresis loop, reversible magnetization curves can be divided into two broad categories.[9] The first type consists of straight lines where the slope increases as the reversing field increases. In this case η is always negative and becomes increasingly negative as the reversing field is increased. This first type of behavior is the result of reversible magnetization arising from rotation of the magnetic moments of the sample out of the easy axis and indicates that domain walls play little part in the reversible magnetization component. This first type of reversible magnetization curve is seen in idealized Stoner-Wohlfarth[7] particles.[9] In the second type of behavior the reversible magnetization curves exhibit a minimum η measured at the positive M_{irr} end point as a function of reversing field is initially positive, passes through zero and becomes negative only in higher fields. This second type of behavior is associated with domain wall bowing being the predominant mechanism giving rise to reversible magnetization and indicates that domain wall motion plays a significant part in the reversal process.[12]

For the initial curves the same two broad categories exist.[9] In the first category of behavior, where M_{rev} arises from rotation of magnetic moments, both the reversible magnetization curves and η are similar to those measured on the hysteresis loop for the same mechanism. The behavior for the second category when domain wall bowing is the dominant reversible magnetization mechanism, is different on the initial curve compared to that seen on the hysteresis loop. In this case the reversible magnetization curves are bowed downward, often quite steeply, η becomes large and negative, and may even approach a value of -1.[13] For materials with a distribution of single domain and multidomain grains, often both types of behavior are seen in different field ranges, η is large and negative in low fields where wall motion is dominant, then becomes smaller, but still negative, when rotation takes over as the dominant reversible magnetization mechanism.

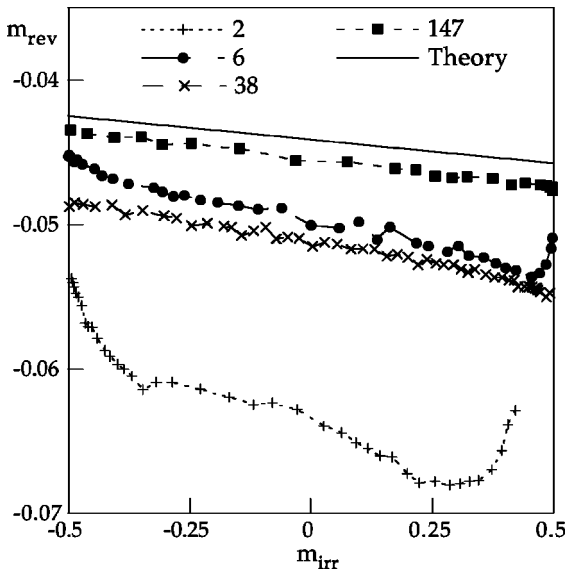

FIG. 5. Reduced reversible magnetization ($m_{rev}=M_{rev}/M_s$) as a function of reduced irreversible magnetization ($m_{irr}=M_{irr}/M_s$) for the four samples studied and an idealized isotropic ensemble of Stoner-Wohlfarth (Ref. 7) particles (''theory'') along the major hysteresis loop, measured and calculated as described in the text. The paramagnetic contribution from the Nd matrix has been subtracted.

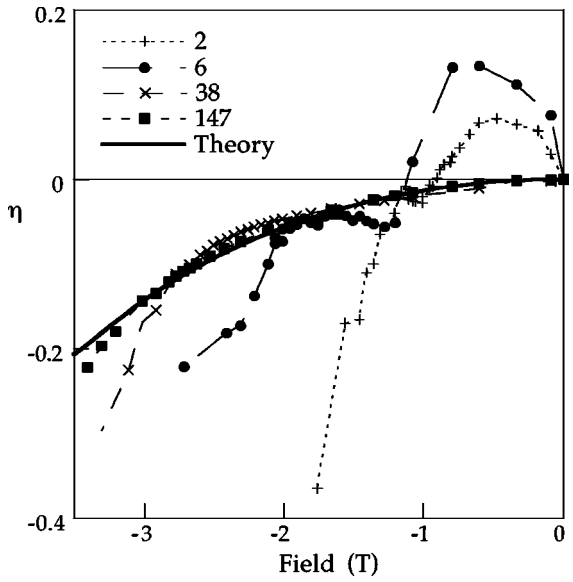

FIG. 6. The variation of η along the major hysteresis loop of the four samples studied, compared with an idealized isotropic ensemble of Stoner-Wohlfarth (Ref. 7) particles (''theory''). Lines are shown as a guide to the eye.

The reversible magnetization curves on the hysteresis loop are shown in Fig. 5 for a field of -5 kOe, as well as an idealized curve for coherently rotating particles. These curves vary depending on the degree of separation between the $Nd_2Fe_{14}B$ particles. For the least dilute samples, 2 and 6, the reversible magnetization curves exhibit a minimum. For the most dilute samples, 38 and 147, the curves become straight lines with a negative slope. The curve for sample 147 is almost identical to the theoretical coherently rotating particle curve. The value of η as the field is changed is shown in Fig. 6 for all four samples, together with the idealized behavior for coherent rotation. As the dilution of the particles is increased the behavior of η approaches that of idealized coherent rotation until for sample 147 the experimentally measured and theoretical curves are almost identical. These results are comparable to the results obtained by Woodward *et al.*[6] on substantially similar samples. Sample 147 is the first sample measured to display such near ideal behavior. A change in behavior of this form, from one displaying domain wall motion to one displaying rotational behavior, has been observed previously in a sintered sample of PrFeB as a function of temperature by Crew *et al.*[14] This change in behavior was explained in that work in terms of the reducing importance of magnetostatic interactions to the reversal process as the temperature decreased.[14] The increasing dilution of the samples in this work is likely to lead to a similar decreasing importance of magnetostatic interactions in the reversal mechanism and result in a similar change in reversal behavior. The change in reversal behavior as interactions are decreased suggests that magnetostatic interactions are responsible for the domain wall processes observed in samples 2 and 6.

Reversible magnetization curves taken from the initial curve are shown for a field of -5 kOe in Fig. 7. These curves are similar to curves measured on the initial curve of melt-quenched NdFeB.[9] The η curves for the initial curve for all four samples, shown in Fig. 8, are also similar to the melt-quenched materials in that they show large negative values of η, up to -0.5. The maximum magnitude of η increases as the dilution increases, because more multidomain grains are present in the more dilute samples, as seen

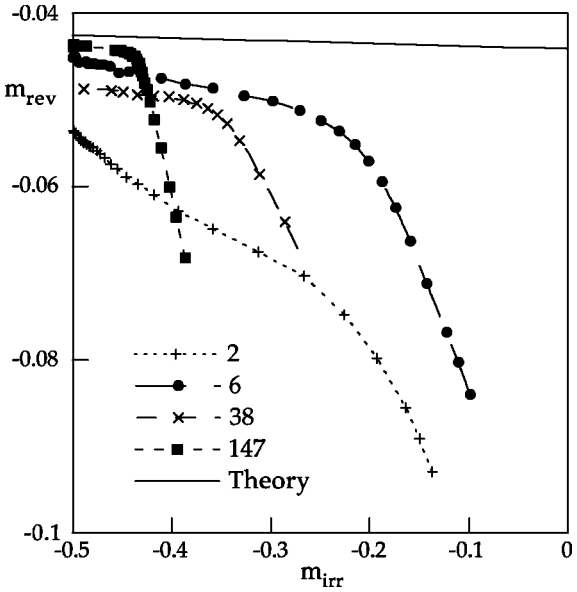

FIG. 7. Reduced reversible magnetization ($m_{rev}=M_{rev}/M_s$) as a function of reduced irreversible magnetization ($m_{irr}=M_{irr}/M_s$) along the initial curve for the four samples studied and an idealized isotropic ensemble of Stoner-Wohlfarth (Ref. 7) particles (''theory''), measured and calculated as described in the text. The paramagnetic contribution from the Nd matrix has been subtracted.

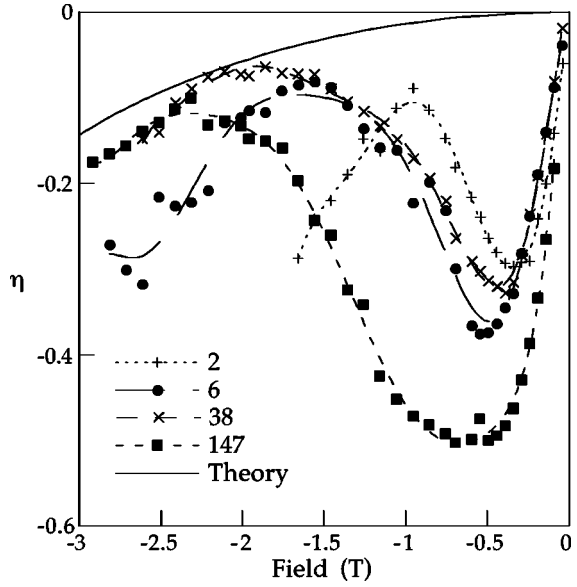

FIG. 8. The variation of η along the initial curve for the four samples studied compared with idealized isotropic ensemble of Stoner-Wohlfarth (Ref. 7) particles (''theory''). Lines are shown as a guide to the eye.

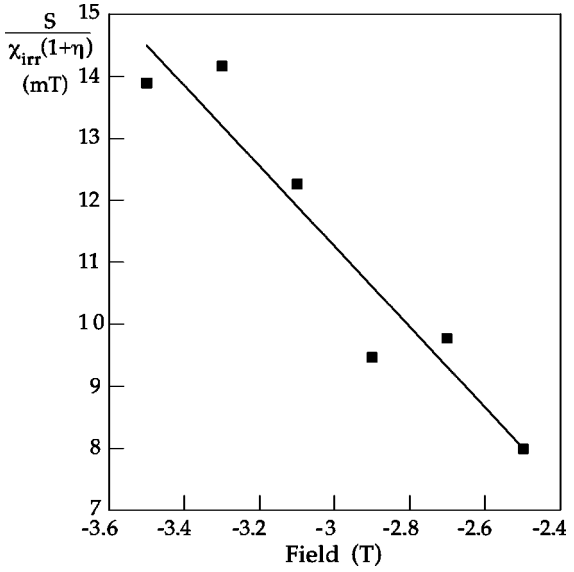

FIG. 9. The variation of $S/\chi_{irr}(1+\eta)$ as a function of field for sample 147. The line is shown as a guide to the eye.

from the initial curves in Fig. 3. This increases the domain wall area and allows more reversible domain wall movement to occur. On the initial curves η is indicating the fraction of material reversed by reversible domain wall motion compared with the fraction reversed when a domain wall is removed from within a grain. For sample 147 η approaches -0.5 as a maximum, which indicates that, on average, domain walls move half as far reversibly as they move irreversibly when annihilated.

3. Magnetic viscosity

For the most dilute composition, sample 147, magnetic viscosity measurements were performed on the major hysteresis loop. These measurements consist of saturating the sample in a large positive field, quickly applying a negative reversing field, and recording the time dependence of magnetization as the field is held constant. The magnetization was recorded for a period of 20 min at a variety of different fields along the major hysteresis curve. For this sample the decay of magnetization (M) in a constant field (H) can be approximated by a logarithmic function of time (t) of the form

$$M(t)=A+S\ln(t+t_0), \tag{2}$$

where A and t_0 are constants and S describes the logarithmic rate of change of magnetization with time. The irreversible susceptibility (χ_{irr}) was calculated from the recoil curves measured previously using the dc demagnetizaton (DCD) method,[15] and the activation volume for reversal (V_{act}) was then calculated from the expression

$$V_{act}=\frac{kT\chi_{irr}(1+\eta)}{SM_s}, \tag{3}$$

where k is Boltzmann's constant, T the temperature, M_s the spontaneous magnetization, and η is the parameter which describes the dependence of M_{rev} on M_{irr} defined in Eq. (1), which is required to correct for reversible magnetization changes during magnetic viscosity. This correction must be applied if true values of V_{act} are to be measured.[15]

The value of the magnetic viscosity parameter,[15] $S/\chi_{irr}(1+\eta)$ as a function of the applied field is shown in Fig. 9. The average value of the viscosity parameter agrees with that obtained by Woodward *et al.*[6] on a similar sample using a different method.[16] Using this parameter, and Eq. (3), the activation volume V_{act} was found to correspond to a sphere between 7.6 and 9.2 nm in diameter. This is considerably smaller than the particle size in this sample.[5] The trend in the viscosity data, a steep increase in the viscosity parameter as the reversing field is increased, is consistent with that predicted for an ensemble of non-interacting isotropic Stoner-Wohlfarth particles.[15] This behavior was explained by the fact that as the field is increased the orientation of the particles which reverse at that field changes[15] which results in the magnetic viscosity parameter increasing with field.

4. Temperature dependence of coercivity

In the theory of micromagnetism the coercive field H_c of a permanent magnet can be described by an extended version of Brown's expression for the nucleation field, H_N,[17]

$$H_c=\alpha_K\alpha_\psi H_N-N_{eff}M_s, \tag{4}$$

where α_K, α_ψ and N_{eff} are microstructural parameters which account for the non-ideal reversal mechanism, including reduced crystal anisotropy at the surface of the grains (α_K), misalignment of the grains (α_ψ), and the strong local demagnetization field at the edges and corners of the grains (N_{eff}). For randomly oriented magnetic grains, as in the samples in this work, $\alpha_\psi=\alpha_\psi^{min}=0.5$ and $\alpha_\psi H_N=H_N^{min}$. In

magnetic materials with non-vanishing high order anisotropy constants (such as $Nd_2Fe_{14}B$), H_N^{min} can be calculated as $(K_1+K_2)/M_s$.[17] The values for anisotropy constants K_1 and K_2 were taken from Hock and Kronmuller.[18] Equation (4) can then be written as

$$H_c/M_s = \alpha_K H_N^{min}/M_s - N_{eff}. \quad (5)$$

Thus the microstructural parameters, α_K and N_{eff}, can be derived from the linear dependence of H_c/M_s versus H_N/M_s. Shown in Fig. 10(a) is the linear dependence of H_c/M_s on H_N/M_s in the temperature range from 190 to 540 K for samples 2 and 6 while Fig. 10(b) shows a similar plot in the temperature range from 100 to 540 K for sample 147. The variation for sample 38 is similar to that for sample 147 shown in Fig. 10(b). The microstructural parameters, α_K and N_{eff} from Eq. (5) for the four samples are shown in Table II. In $Nd_2Fe_{14}B$ the second anisotropy constant K_2 exceeds K_1 below 190 K, associated with a spin reorientation, causing deviation from linear dependence below 190 K, which is shown for sample 147 in Fig. 10(b). Above 490 K an abrupt decrease in coercivity of samples 38 and 147 causes a nonlinear dependence of H_c/M_s.

Regarding the temperature dependence of coercivity and the micromagnetic parameters calculated and shown in Table II, it can be noted that α_K increases with an increase in the Nd concentration. For samples 38 and 147, $\alpha_K \approx 1$, which is most likely due to the perfect surface of the $Nd_2Fe_{14}B$ grains in these samples as observed by TEM.[5] A perfect surface is without inhomogeneities which would reduce the magnetocrystalline anisotropy at the surface and hence the coercivity. The value of N_{eff} first increases with the Nd concentration, reaching the largest value for sample 38, and then decreases slightly in sample 147. TEM observations show that the shape of the $Nd_2Fe_{14}B$ grains changes from polyhedral in samples with low Nd concentration, to plate-like for high Nd concentration.[5] These platelike $Nd_2Fe_{14}B$ grains have the crystallographic *c* axis aligned normal to the plate. Thus the demagnetization factor of these grains is large and negative, $N=N_{\parallel}-N_{\perp}=-0.48$.[4] The increase in N_{eff} with increasing Nd content is due to the change in shape of the constituent grains. The shapes of the $Nd_2Fe_{14}B$ grains in samples 38 and 147 are similar, however. Moreover, the $Nd_2Fe_{14}B$ grains in these samples are randomly distributed in the Nd-rich matrix. The magnetostatic interparticle interactions, which also contribute to N_{eff}, decrease with the increase in Nd concentration in these two samples. This could explain the decrease of N_{eff} in sample 147 as compared with sample 38.

For sample 2 the value of N_{eff} is much lower than that in the other three samples measured. This is probably due to the absence of nonmagnetic inclusions in this sample, which are known to increase N_{eff}. Also the grain shape is more nearly spherical in this sample, compared with the plate-like grain shape in the other samples, which is likely to increase N_{eff} relative to sample 2.

C. Modeling

In order to understand the effect of interactions on the reversal of these dilute systems it is important to understand the reversal mechanism of isolated particles. To this end two micromagnetic models were used to examine the reversal of particles typical of those found in samples 38 and 147.

The first model used was a two dimensional model based on the Object Oriented MicroMagnetic Framework (OOMMF) software available from NIST.[19] In the OOMMF model three-dimensional spins are arranged on a two-dimensional mesh and relaxed using a Landau-Lifshitz ordinary differential equation solver[20] with a damping constant of 0.5. The $Nd_2Fe_{14}B$ particle was modeled as a rectangular

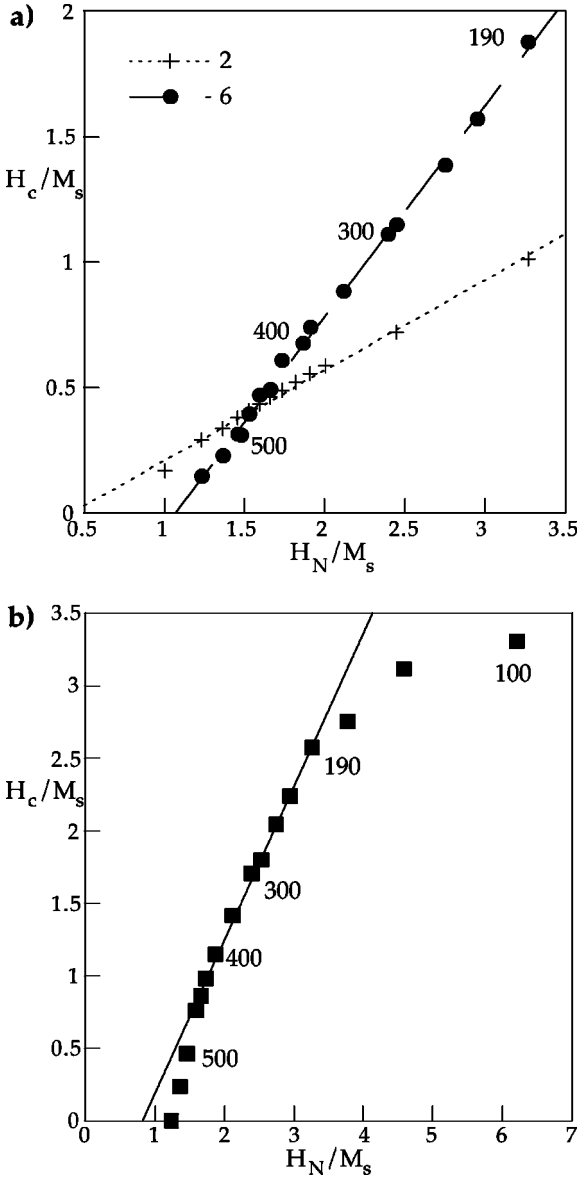

FIG. 10. H_c/M_s as a function of H_N/M_s. (a) For samples 2 and 6. The lines shown are lines of best fit to the data. The temperature of measurement is indicated on the plot for sample 6. (b) For sample 147, showing the nonlinear behavior at low temperature (due to the spin reorientation at 135 K) and at temperatures above 490 K. The line of best fit in this plot is only for data between 190 and 490 K. The temperature of measurement is indicated on the plot. Sample 38 (not shown) displayed a similar nonlinear behavior at high temperature.

TABLE II. Micromagnetic characterization parameters α_K and N_{eff}.

Sample label	α_K	N_{eff}
2	0.36	0.15
6	0.84	0.90
38	0.98	0.93
147	1.06	0.87

parallelepiped of size $100\times40\times25$ nm^3 ($a\times b\times c$) with material properties $K=5$ MJ/m^3, $A=10$ pJ/m, and $M_s=1274$ kA/m. This is the size and shape of particles observed in sample 147 by TEM.[5] The cell size chosen was 1.5 nm, sufficiently small to allow a modeling of the 4.5-nm-wide domain walls in this system. Some calculations were performed with a cell size of 0.25 nm which yielded the same results as those with a larger cell size. The *c* axis, which is the easy axis in this system, was modeled both in the plane of the simulation as well as out of the plane. Results for the value of coercivity were similar to within 5% regardless of the geometry. The field was applied at angles between 0 and 90° to the *c* axis.

Coercivities were calculated for particles similar to those in sample 147 as a function of the applied field angle. The coercivities were consistently 10% below that expected from coherent rotation,[7] including only the magnetocrystalline anisotropy of the particle. The values of coercivity calculated as a function of the angle between the field and the easy axis for one particular geometry, using the OOMMF model, are shown in Fig. 11 and compared with that expected for coherent rotation, normalized to the anisotropy field used in the model of 7.8 T. Most, but not all, of the difference between the model results and Stoner-Wohlfarth theory, can be credited to the effect of shape anisotropy of the particle, which lowers the effective anisotropy field by approximately 0.58 T or 7.5%.[5] One criticism of these results is that it might be expected that the values of coercivity obtained from this model represent lower bounds on the coercivity, compared to the values which would be obtained in a full 3 dimensional model, because of the tendency of two-dimensional models to overestimate the demagnetizing field effects.[21] In the OOMMF model however, the spins are able to orient in 3 dimensions and this makes the OOMMF results close to those obtained with a full three-dimensional model. Indeed, a full 3 dimensional treatment for limited orientations of the field to the easy axis returned similar values for the coercivity. It is therefore expected that for a randomly oriented ensemble of particles of the geometry seen in sample 147 that the coercivity will decrease approximately 10% compared with the ideal Stoner-Wohlfarth theory. The decrease in coercivity compared with idealized theory, even including shape effects, arises because the actual reversal of the particle consists of nucleation of a reverse domain at both the top and the bottom surfaces, which then expands to reverse the whole particle. To confirm this picture of the mechanism of reversal a full three-dimensional treatment of the particle reversal was modeled.

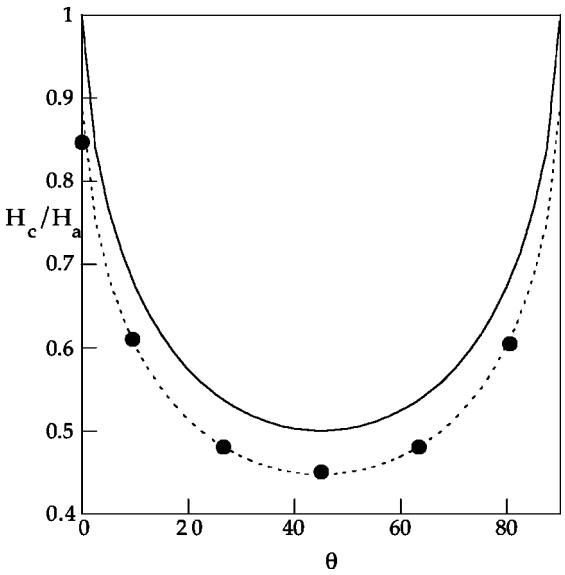

FIG. 11. Micromagnetic modeling results for coercivity as a function of applied field angle θ for particles of similar shape to those in sample 147 ($a\times b\times c=100\times40\times25$ nm^3). The points indicate the coercivity calculated from the two-dimensional model, the solid line the coercivity expected from Stoner-Wohlfarth coherent rotation theory, and the dotted line to coercivities equal to 90% of that expected from Stoner-Wohlfarth coherent rotation theory. The plane modeled was that containing the a and *c* axes of the particle, with the applied field in the same plane. The *c* axis is the easy axis in this system. A full three dimensional modeling treatment returned coercivities very similar to those shown for the two-dimensional model.

In the full three-dimensional treatment the time evolution of the magnetization again follows the Landau-Lifshitz equation of motion,

$$\frac{d\boldsymbol{M}}{dt}=-\gamma_0\boldsymbol{M}\times\boldsymbol{H}_{eff}+\frac{\alpha}{M_s}\boldsymbol{M}\times\frac{\partial\boldsymbol{M}}{\partial t}, \tag{6}$$

which describes the physical path of the magnetization **M** toward equilibrium. γ_0 is the gyromagnetic ratio of the free electron spin and α is the damping constant, taken to be 1. The value of α taken for the three dimensional treatment was different to that assumed for the OOMMF modeling to allow a faster convergence, but the coercive fields were found to be insensitive to the value of α chosen. The effective field $\boldsymbol{H}_{eff}$ is the negative functional derivative of the total magnetic Gibb's free energy, which can be expressed as the sum of the exchange energy, the magneto-crystalline anisotropy energy, the magnetostatic energy, and the Zeeman energy.[22] To solve the Gilbert equation numerically the magnetic particle was divided into finite elements. A hybrid finite element boundary element method[23] was used to calculate the scalar potential *u* on every node point of the finite element mesh. The demagnetizing field, which contributes to the effective field, was taken as the negative derivative of the scalar potential *u*. The effective field $\boldsymbol{H}_{eff,i}$ at the node point i of an irregular finite element mesh was approximated using the box scheme

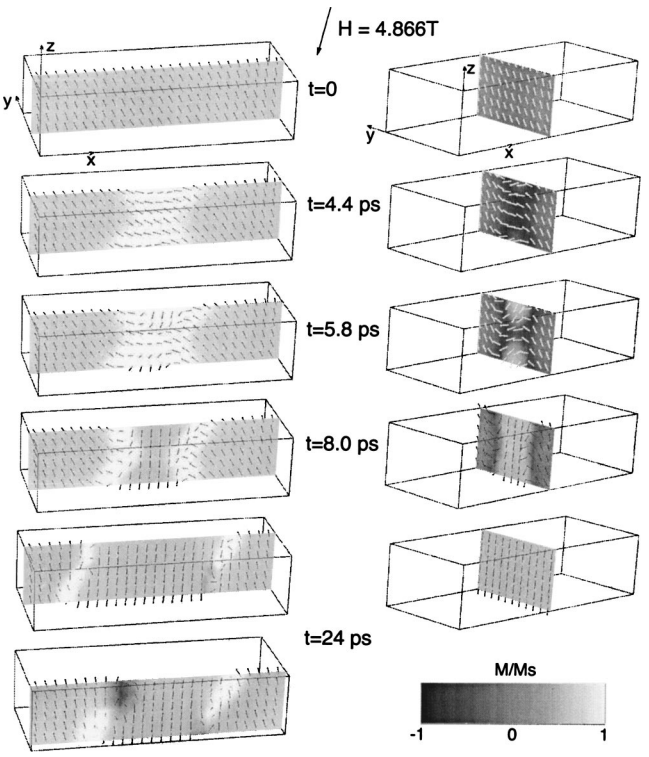

FIG. 12. Simulated magnetic reversal in a constant field of a particle similar to that observed in sample 147. The external field is applied in the $H_x=-1$, $H_y=0$, and $H_z=-6$ directions. The two upper pictures show the magnetization immediately after the field was increased from 4.787 to 4.866 T, which is equal to the coercive field. Also shown in the upper pictures are the *x*, *y*, and *z* directions. The arrows show the projection of the magnetization onto the shaded plane. The perpendicular component of the magnetization is shaded according to the key at bottom right. The bottom left picture shows the magnetization state near the surface of the particle 24 ps after the field was increased.

$$\boldsymbol{H}_{eff,i}=-\left(\frac{\partial E_i}{\partial \boldsymbol{M}}\right)_i=-\frac{1}{V_i}\frac{\partial E_i}{\partial \boldsymbol{M}_i},\quad \text{for } V_i\to 0, \tag{7}$$

where V_i is the volume of the surrounding node *i*, such that

$$\sum_i V_i=V \quad \text{and} \quad V_i\cap V_j=0 \quad \text{for} \quad i\neq j. \tag{8}$$

The space discretization of the Landau-Lifshitz equation leads to three ordinary differential equations for every node. In the case of a stiff problem a backward differentiation formulas is used for the time integration, which leads to a system of nonlinear equations. After applying Newton's method the resulting system of linear equations is solved using the scaled generalized minimal residual method.[24]

The process of reversal in the full three-dimensional micromagnetic model is shown in the series of micromagnetic states in Fig. 12. This figure is a time series of the reversal in a constant field and the states shown are not equilibrium states. In Fig. 12 an external field is applied in the $H_x=-1$, $H_y=0$, and $H_z=-6$ direction as indicated in the figure. The time $t=0$ is immediately after the field was increased from 4.787 to 4.866 T, which is equal to the coercive field for this particle. Figure 12 shows the nonideal nature of the reversal, with nucleation of a reverse domain occurring at the top and bottom surfaces of the particle.

D. Discussion

1. Coercivity and packing fraction

From Fig. 2(a) the coercivity is plainly not linear with the packing fraction over the full range of packing fractions investigated. Sample 2, which is close to stoichiometric $Nd_2Fe_{14}B$, has a markedly lower coercivity than the other samples. This is due to the large amount of exchange interactions which are present between grains in this sample. The reversible magnetization measurements show the presence of stable domain walls during magnetization reversal. Two mechanisms can lead to stable domain walls in high reversal fields in the absence of pinning sites within the grains. Magnetostatic interactions at grain corners can stabilize domain walls to quite high fields, as was shown in sintered PrFeB samples.[14] However, from Table II the value of N_{eff} is low in sample 2 so magnetostatic effects are likely to be small. Exchange interactions across grain boundaries can also stabilize domain walls as seen in melt-quenched NdFeB.[9] Significant intergranular exchange interactions in this sample are consistent with the substantially lower value of α_K observed, compared with the more dilute samples. In addition the micromagnetic parameters shown in Table II for sample 2 are substantially lower than the other, more decoupled, samples. Most notably, α_K is lower indicating a substantially different reversal process. The lower coercivity of this sample compared with the Nd rich samples is in accord with previous results in which small additions of Nd above stoichiometry improves the coercivity.[25,26]

Sample 6, together with the samples taken from other work shown in Fig. 2(a), form a second regime of coercivity as a function of packing fraction. The reversible magnetization measurements of Figs. 5 and 6 together with the two steps on the initial curve in Fig. 3 show that sample 6, compared with the highly diluted samples (38 and 147), has a different reversal mechanism, which includes domain wall motion. This is most likely due to a clustering of grains within the sample which leads to the grains not being completely exchange decoupled. Clustering of grains also leads to a smaller increase in coercivity with decreasing packing fraction than expected from the overall bulk composition of the sample.

In samples 38 and 147, the coercivity increases faster as the packing fraction is decreased than for less dilute samples. The reversible magnetization measurements for these samples indicate a nonuniform reversal of individual grains suggesting that full exchange decoupling has been achieved. The increasing coercivity with dilution arises because of the decreasing importance of intergranular magnetostatic interactions. It is only in this region that the relationship of Néel and Wohlfarth would be expected to be obeyed.

There is one further influence on the coercivity which is not due purely to clustering of grains. The TEM measurements of Girt *et al.*[5] showed that the size and shape of the

grains changes as the packing fraction is decreased. The grains for high packing fractions are polyhedral and equiaxed. For lower packing fractions the grains become elongated parallelepipeds with the axis ratio changing with the Nd concentration. It is difficult to quantify this effect of the changing shape, and thus ''correct'' the measured coercivity values because an exact description of the shapes of the grains is not available. The effect is likely to be a small, but not negligible, change in coercivity. An estimate for the size of this effect, based on the shape demagnetization factor for sample 147 gives a ''shape anisotropy'' of approximately 0.3 T, which is 10% of the measured coercivity. This factor will be less for samples with lower Nd contents as the shape of the grain changes to a more spherical one. This shape correction is not large enough to make the coercivity plot of Fig. 2(a) linear.

Once saturated, at room temperature the grains in sample 147 never again have stable domain walls within them, as evidenced by the reversible magnetization results. Despite the single domain reversal process of the grains in this sample, the coercivity is still some 20% below that expected for idealized coherent rotation. The reduction in coercivity for these grains compared with theory is a result of a number of factors, the magnitudes of which can only be estimated. Firstly the reversal mechanism of these grains is not coherent rotation, as shown clearly by the micromagnetic modeling results of Fig. 12, but is instead a process in which reverse domains nucleate within the grain and subsequently reverse the whole grain. The micromagnetic modeling suggest that this reversal mechanism, compared with idealized coherent rotation, results in a decrease in coercivity of approximately 10%, equivalent to 0.4 T. This estimate includes the reduction expected because of the shape anisotropy of the particle. The reversal mechanism is not coherent rotation because the particle size is much larger than the size for which coherent rotation is the preferred reversal mode, estimated to be approximately 10 nm in most materials.[27] The reversal mechanism pictured in Fig. 12 is supported by the similar sizes for the nucleus of reverse magnetization and the calculated activation volume determined from time dependence measurements.

Thermal activation will reduce the coercivity further compared with that expected from the micromagnetic modeling results. Estimating from the values of the magnetic viscosity parameter measured in Fig. 9, the reduction in coercivity from thermal activation will be

$$\Delta H = \frac{25nS}{\chi_{irr}(1+\eta)}, \tag{9}$$

where n is the power of the reduced field H/H_k which is assumed to be the dominant term in the description of the variation of the energy barriers to reversal with magnetic field.[28] For randomly oriented particles a power of 3/2 is often taken[29] which results in a measured coercivity decrease of 0.38 T.

The value of coercivity for idealized coherent rotation in isotropic $Nd_2Fe_{14}B$ is 3.6 T. In sample 147 the nonideal reversal mode and thermal activation of reversal lead to a reduction in coercivity of 0.78 T. The predicted coercivity is thus 2.82 T, which when compared to the measured coercivity of 2.83 T is a remarkably close agreement.

2. Reversal mechanism

In the least dilute samples, 2 and 6, the reversal mechanism consists of domain wall motion, evidenced by the reversible magnetization measurements in Figs. 5 and 6. In samples 38 and 147 reversal is by a nonuniform mode of individual grains.

Despite the differences between the samples in magnetization reversal behavior on the demagnetization curve, the initial curve behavior is similar, with domain walls present after thermal demagnetization in all samples. In samples 38 and 147 the presence of domain walls on the initial curve means that the absence of domain walls on the demagnetization curve is not because the $Nd_2Fe_{14}B$ particles in these two samples cannot support domain walls, but rather is because the dynamics of the reversal are different in these dilute samples compared with samples 2 and 6.

Careful examination of the initial curves in Fig. 3 reveals that for all samples there are two steps on the curve. The second step appears at a field which is close to the coercive field of that sample on the major hysteresis loop. In the less dilute samples, 2 and 6, where intergranular exchange coupling is suggested, this second step is most likely due to the unpinning of domain walls from grain boundaries. In these less dilute samples the second step is quite large, indicating a significant fraction of the material reverses in this way. For the most dilute samples, 38 and 147, due to the absence of intergranular exchange interactions, this second step on the initial curve most likely corresponds to the reversal of single domain grains. The second step is much smaller than the first step on the curve, suggesting that in these dilute samples only a small fraction of the grains are single domain in the thermally demagnetized condition.

For the less dilute samples, 2 and 6, the presence of stable domain walls during reversal at the fields new domain walls are nucleated on the demagnetization curve, suggests there exist pinning sites strong enough to prevent the motion of these domain walls. In the absence of pinning sites within the grains, the presence of sufficiently strong pinning sites must be due to intergranular interactions, especially exchange interactions in sample 2 but including magnetostatic interactions in sample 6, evidenced by the larger value of N_{eff} for this sample in Table II. The intergranular interactions lower the nucleation fields while simultaneously allowing the grain boundaries to become pinning centers.[30,31] The strength of the intergranular pinning centers is indicated by the position of the second step on the initial curves in Fig. 3. For the most dilute samples, 38 and 147, the grain boundaries cannot act as pinning centers because of the lack of sufficiently strong intergranular interactions. In addition the absence of intergranular exchange interactions raises the nucleation fields such that any pinning sites which might exist within the grains are too weak to prevent subsequent domain wall motion.

In summary, the reversal mechanism for the least dilute samples, 2 and 6, is domain wall motion and pinning on both

initial and demagnetization curves. The pinning is hypothesized to result from intergranular exchange and magnetostatic interactions. In contrast, the most dilute samples, 38 and 147, contain no substantial pinning sites, because of the lack of intergranular interactions, and reverse via a nucleation mechanism.

3. Domain walls on the initial curve

The presence of domain walls on the initial curve for all samples is somewhat in contradiction to the small particle size observed by transmission electron microscopy.[5] In the less dilute samples, 2 and 6, the $Nd_2Fe_{14}B$ grains are well below the single domain limit of 200–300 nm in $Nd_2Fe_{14}B$.[32,33] However, similar to other fine-grained Nd-FeB magnets, domain walls can be supported across a number of grains because of the intergranular interactions which are present.[31] The domains which are formed in this way are known as interaction domains. For the most dilute samples, 38 and 147, strong intergranular interactions are absent and a different explanation is required for the observed presence of domain walls on the initial curve.

Using the three-dimensional micromagnetic model, it is possible to calculate the energy of particles similar in size and shape to those in samples 38 and 147, with and without the presence of the domain wall. The magnetostatic self energy of such a particle is 53×10^{-18} J. The total energy of a particle with a domain wall present, in the configuration shown in Fig. 4, is 66×10^{-18} J, consisting of a magnetostatic self-energy of 39×10^{-18} J and a domain wall energy of 27×10^{-18} J. Thus a multidomain particle has an energy some 25% higher than a single domain particle. Why then does such a particle take up a multi-domain state following thermal demagnetization? The answer lies in considering the energy barrier between these two states.

To move a domain wall out of a multidomain particle requires overcoming an energy barrier resulting from the increase in magnetostatic energy during the domain wall translation. This energy barrier can be estimated as 14×10^{-18} J, being the difference in magnetostatic energy of the multi-domain and single domain configurations. This is equivalent to 3400 kT at room temperature, which means that a particle in the metastable multidomain state is in a very deep energy minimum. At higher temperatures this energy barrier drops sharply (e.g., the barrier is 900 kT at 500 K) because it scales with M_s^2 as well as the temperature.

An estimate of the field stability of the two domain state is 0.12 T, calculated as the field that is required in order for the Zeeman energy to be equivalent to the energy barrier. Detailed modeling with both the two- and three-dimensional models gave a higher stability field of 0.28 T, which is larger because of the detailed calculation of the magnetostatic energy as a function of wall position. The results of the models in this case however, are somewhat sensitive to the details of the magnetization configuration in the domain wall.

To investigate the likelihood of the multidomain state arising during cooling from the Curie temperature, a simulated cooling procedure was undertaken using the three-dimensional micromagnetic model, in which the micromagnetic elements were initially assigned direction randomly, and the system allowed to evolve to a stable configuration using room temperature material properties. This procedure is formally equivalent to an instantaneous quench from above the Curie Temperature to room temperature. The evolution of the magnetization configuration for one such run is shown in Fig. 13. From the result of 20 simulated runs it was determined that the single domain state was reached in only 35% of the simulations. The rest of the simulations (65%) became stable in a multidomain state, with the vast majority being a two domain state (50%) although some three- (10%)

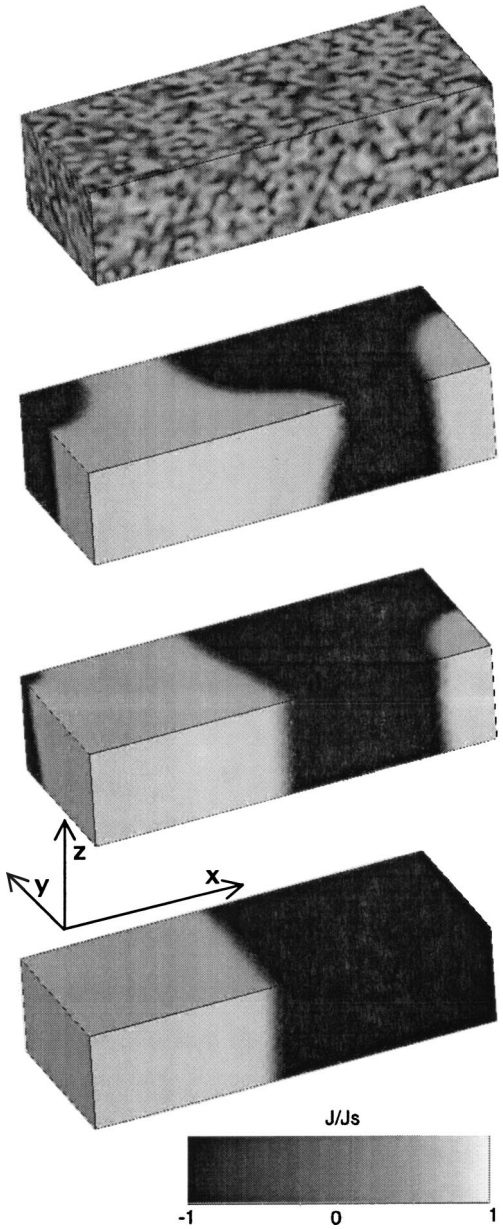

FIG. 13. A simulation of the approach to a stable state. The micromagnetic elements are initially assigned a random direction, and the system is allowed to evolve to a stable state. For this particular run a two domain state is found to be stable, even though a single domain state has a lower energy. The snapshots correspond to the initial state and 0.1, 0.2, and 1 ns after commencing the simulation. The last snapshot is the stable state. The *z* component of magnetization is shaded according to the key shown.

and four- (5%) domain configurations were also found. The proportion of single domain states observed from the simulation is higher than that seen on the initial curve, evidenced by the size of the second step in Fig. 3, but this is a result of using an instantaneous quench rather than using a true simulated cooling from the Curie temperature. The energy barrier between the single domain and multidomain states is much higher at room temperature than at higher temperatures, and thus using room temperature properties in the simulation will more favorably predispose the system to stabilize in the single domain state compared with the experimental cooling regimen.

The important implication of this study is that thermal demagnetization of magnetic samples does not guarantee that the system is subsequently in a global energy minimum state. This has implications for the interpretation of initial curves because the system may be in a metastable state, rather than a global minimum of energy. It may be presumed that the global minimum energy state can be reached by cooling through the Curie temperature sufficiently slowly, but how slowly is required for the system to be ergodic has not been determined.

E. Conclusion

Reversible magnetization measurements, micromagnetic modeling, the temperature dependence of coercivity, and magnetic viscosity measurements have been used to clarify the magnetic reversal mechanism of $Nd_2Fe_{14}B$ particles diluted to various extents in a Nd matrix. Dilution of the particles varied from close to zero, for sample 2, to close to 90% of the material being Nd matrix phase, for sample 147.

The coercivity was observed to increase markedly as the dilution of the $Nd_2Fe_{14}B$ phase was increased. The increase in coercivity was accompanied by a change in the reversal mechanism. In samples 2 and 6, domain wall motion involving several grains governed by intergrain interactions was active. In samples 38 and 147 nonuniform reversal of individual grains was dominant, reversal occurring particle by particle and resembling the behavior of isolated Stoner-Wohlfarth particles. The value of the coercivity in sample 147 was in excellent agreement with micromagnetic modeling results for isolated particles once the effect of thermal activation of magnetization reversal was accounted for.

The initial magnetic state after thermal demagnetization was found in all samples, regardless of dilution, to be one in which a substantial proportion of grains contained domain walls. Micromagnetic simulations showed, for sample 147, that the single domain state is the lowest energy state. It was concluded that thermal demagnetization does not result in the material assuming a global energy minimum, but rather the system remains in a local metastable energy minimum. Micromagnetic calculations revealed a significant energy barrier for the removal of a domain wall within the grain once it is formed.

ACKNOWLEDGMENTS

The 2D micromagnetic modeling code used in this work, the Object Oriented MicroMagnetic Framework (OOMMF), was developed and distributed by NIST. This research was performed in part under the auspices of the U.S. Department of Energy, Division of Material Sciences, Office of Basic Energy Sciences under Contract Nos. DE-AC02-98CH10886 and DE-AC03-76SF00098, and was partly supported by the Austrian Science Fund (Y-132 PHY). DCC would like to thank Dr. Robert Woodward and Dr. Robert Stamps for valuable discussions.

*Corresponding author. Email address: dcrew@physics.uwa.edu.au

[1] L. Néel, Acad. Sci., Paris, C. R. **224**, 1550 (1947).
[2] E.P. Wohlfarth, Proc. R. Soc. London, Ser. A **232**, 208 (1955).
[3] M. El-Hilo, R.W. Chantrell, and K. O'Grady, J. Appl. Phys. **84**, 5114 (1998).
[4] Er. Girt, K.M. Krishnan, G. Thomas, and Z. Altounian, Appl. Phys. Lett. **76**, 1746 (2000).
[5] Er. Girt, K.M. Krishnan, G. Thomas, E. Girt, and Z. Altounian, J. Magn. Magn. Mater. **231**, 219 (2001).
[6] R.C. Woodward, N.T. Gorham, R. Street, D.C. Crew, E. Girt, and K.M. Krishnan, IEEE Trans. Magn. **37**, 2493 (2001).
[7] E.C. Stoner and E.P. Wohlfarth, Philos. Trans. R. Soc. London, Ser. A **240**, 599 (1948).
[8] Er. Girt, K.M. Krishnan, G. Thomas, Z. Altounian, and M. Dikeakos, J. Appl. Phys. **88**, 5311 (2000).
[9] D.C. Crew, P.G. McCormick, and R. Street, J. Appl. Phys. **86**, 3278 (1999).
[10] R. Skomski and J.M.D. Coey, *Permanent Magnetism* (Institute of Physics Publishing, Bristol, 1999), p. 298.
[11] R.C. Cammarano, P.G. McCormick, and R. Street, J. Phys. D **29**, 2327 (1996).
[12] D.C. Crew, R.C. Woodward, and R. Street, J. Appl. Phys. **85**, 5675 (1999).
[13] D.C. Crew, P.G. McCormick, and R. Street, Appl. Phys. Lett. **74**, 591 (1999).
[14] D.C. Crew, L.H. Lewis, D.O. Welch, and F. Pourarian, J. Appl. Phys. **87**, 4744 (2000).
[15] D.C. Crew, S.H. Farrant, P.G. McCormick, and R. Street, J. Magn. Magn. Mater. **163**, 299 (1996).
[16] L. Folks and R. Street, J. Appl. Phys. **76**, 6391 (1994).
[17] G. Martinek and H. Kronmuller, J. Magn. Magn. Mater. **86**, 177 (1990).
[18] S. Hock and H. Kronmuller, in *Proceedings of the* 5^{th} *International Symposium of Magnetic Anisotropy and Coercivity in Rare Earth-Transition Metal Alloys*, edited by C. Herget, H. Kronmuller and R. Poerschke (Deutsche Physikalische Gesellschaft, Bad Honnef, 1987), p. 275.
[19] M.J. Donohue and D.G. Porter, urlhttp://math.nist.gov/oommf/ version 1.1
[20] M.J. Donahue and D.G. Porter, OOMMF User's Guide, Version 1.0, National Institute of Standards and Technology Technical Report No. NISTIR 6376, 1999 (unpublished).
[21] T. Schrefl, J. Fidler, and H. Kronmuller, J. Magn. Magn. Mater. **138**, 15 (1994).
[22] W.F. Brown, Jr., *Micromagnetics* (Wiley, New York, 1963).
[23] D.R. Fredkin and T.R. Koehler, IEEE Trans. Magn. **26**, 415 (1990).

[24] P.N. Brown and A.C. Hindmarsh, J. Comput. Appl. Math. **31**, 40 (1989).
[25] W.B. Muir, Z. Altounian, T. Gou-hua, and C. Wan-rong, J. Magn. Magn. Mater. **81**, 168 (1989).
[26] I. Ahmad, H.A. Davies, and R.A. Buckley, J. Magn. Magn. Mater. **157/158**, 31 (1996).
[27] R. Skomski, J.P. Liu, and D.J. Sellmeyer, in *Advanced Hard and Soft Magnetic Materials*, edited by M. Coey *et al.*, MRS Symposia Proceedings No. 577 (Materials Research Society, Warrendale PA, 1999), p. 335.
[28] D.C. Crew, P.G. McCormick, and R. Street, J. Phys. D **29**, 2313 (1996).
[29] R. Victora, Phys. Rev. Lett. **63**, 457 (1989).
[30] D.C. Crew, L.H. Lewis, D.O. Welch, and V. Panchanathan, J. Appl. Phys. **87**, 6570 (2000).
[31] D.C. Crew and L.H. Lewis, IEEE Trans. Magn. **37**, 2512 (2001).
[32] J.F. Herbst, Rev. Mod. Phys. **63**, 819 (1991).
[33] D. Givord and M.F. Rossignol, in *Rare-Earth Iron Permanent Magnets*, edited by J. M. D. Coey (Clarendon Press, Oxford, 1996), Chap. 5.